Morphology-Controllable Synthesis of Mesoporous CeO_2 Nano- and Microstructures

Chunman Ho,[†] Jimmy C. Yu,*[,†] Tszyan Kwong,[†] Angelo C. Mak,[†] and Sukyin Lai[‡]

Department of Chemistry and Environmental Science Programme, The Chinese University of Hong Kong, Shatin, New Territories, Hong Kong, China, and Department of Chemistry, Hong Kong Baptist University, Kowloon, Hong Kong, China

Received April 15, 2005. Revised Manuscript Received May 30, 2005

Spherical cerium oxide nanoparticles and microsized rod-shaped and spindle-like CeO_2 structures have been synthesized using a polyol method. When the duration of reaction and the concentration of cerium precursor are controlled, CeO_2 products of different morphologies can be selectively produced. Results from XRD, XPS, SEM, and FT-IR measurements suggest that the CeO_2 nanospheres are formed from the decomposition of the cerium precursor. Further reactions between the as-prepared CeO_2 and ethylene glycol yield the rods/spindle-like cerium formate particles. These morphologies are preserved even after calcination. The order of band gap energy of these samples was found to be rod-shaped > spherical > spindle-like samples, as determined by the UV−Vis spectroscopic method. Compared to a nonoriented polycrystalline CeO_2, these samples show an increase in band gap energy due to the quantum size effect. The higher catalytic activity on CO conversion in a spindle-like sample can be explained from the extent of Ce(IV) reduction and the oxygen vacancy.

1. Introduction

One-dimensional (1D) nanostructures have enormous potential as components of nanodevices and sensors because of their peculiar properties, which originate from their high surface area and low dimensionality.[1] There are many applications where nanostructured materials could be exploited to greatly enhance the functionality or performance of materials.[2] Much effort has been devoted to the synthesis of nanomaterials using various methods.[3] The ethylene glycol-mediated synthesis is known to be one of the most powerful general methods to prepare uniform 1D nanomaterials.[4] Ethylene glycol has been widely used in the polyol synthesis of metal nanoparticles because of its physical properties: (1) a high dielectric constant, which enhances the solubility of inorganic salts; (2) a high boiling point (195 °C at atmospheric pressure), which makes it possible to carry out the preparation of inorganic compounds at relatively high temperatures; and (3) its strong reducing power.

The morphology-controllable synthesis of nanostructured metal compounds including PbSe,[5] ZnO,[6] $In(OH)_3$,[7] SnO_2,[8] and V_2O_5[9] have been successfully developed. CeO_2 possesses many attractive properties which make it highly promising for a wide range of applications such as solid electrolytes in solid oxide fuel cells,[10] automotive three-way catalysts,[11] ultraviolet absorbers,[12] and oxygen sensors.[13] It is also used as a catalyst for large-scale fluid cracking in refineries and dehydrogenation of ethyl benzene to styrene.[14] Nanocrystalline ceria are expected to have superior physical properties. Chiang et al. demonstrated a 4 orders of magnitude increase

* Corresponding author: Prof. Jimmy C. Yu. Fax: (852) 2603 5057. E-mail: jimyu@cuhk.edu.hk.
† The Chinese University of Hong Kong.
‡ Hong Kong Baptist University.

(1) (a) Xia, Y.; Yang, P.; Sun, Y.; Wu, Y.; Mayers, B.; Gates, B.; Yin, Y.; Kim, F.; Yan, H. *Adv. Mater.* **2003**, *15*, 353. (b) Lieber, C. M. *Solid State Commun.* **1998**, *107*, 607. (c) Smalley, R. E.; Yakobson, B. I. *Solid State Commun.* **1998**, *107*, 567. (d) Hu, J.; Li, L. S.; Yang, W.; Mamnna, L.; Wang, L. W.; Alivisatos, A. P. *Science* **2001**, *292*, 2060.
(2) (a) Ahmadi, T. S.; Wang, Z. L.; Green, T. C.; Henglein, A.; El Sayed, M. A. *Science* **1996**, *272*, 1924. (b) Huynh, W.; Peng, X. G.; Alivisatos, A. P. *Adv. Mater.* **1999**, *11*, 923. (c) Mattoussi, H.; Radzilowski, L. H.; Dabbousi, B. O.; Thomas, E. L.; Bawendi, M. G.; Rubner, M. F. *J. Appl. Phys.* **1998**, *83*, 7965. (d) Chan, W. C. W.; Nie, S. M. *Science* **1998**, *281*, 2016.
(3) (a) Patzke, G. R.; Krumeich, F.; Nesper, R. *Angew. Chem., Int. Ed.* **2002**, *41*, 2446. (b) Wang, Z. L. *Adv. Mater.* 2003, *15*, 432.
(4) (a) Wang, Y.; Jiang, X.; Xia, Y. *J. Am. Chem. Soc.* **2003**, *125*, 16176. (b) Jiang, X.; Wang, Y.; Herricks, T.; Xia, Y. *J. Mater. Chem.* **2004**, *14*, 695. (c) Sun, Y.; Xia, Y. *Adv. Mater.* **2003**, *15*, 695. (d) Sun, Y.; Mayers, B.; Xia, Y. *Adv. Mater.* **2003**, *15*, 641. (e) Sun, Y.; Mayers, B.; Xia, Y. *Nano Lett.* **2003**, *3*, 675. (f) Sun, Y.; Mayers, B.; Herricks, T.; Xia, Y. *Nano Lett.* **2003**, *3*, 955. (f) Feldmann, C. *Adv. Funct. Mater.* **2003**, *13*, 101.
(5) Lifshitz, E.; Bashouti, M.; Kloper, V.; Kigel, A.; Eisen, M. S.; Berger, S. *Nano Lett.* **2003**, *3*, 857.
(6) (a) Zhang, J.; Sun, L.; Yin, J.; Su, H.; Liao, C.; Yan, C. *Chem. Mater.* **2002**, *14*, 4172. (b) Vayssieres, L. *Adv. Mater.* **2003**, *15*, 464. (c) Pacholski, C.; Kornowski, A.; Weller, H. *Angew. Chem., Int. Ed.* **2002**, *41*, 1188. (d) Lao, J. Y.; Wen, J. G.; Ren, Z. F. *Nano Lett.* **2002**, *2*, 1287.
(7) Perez-Maqueda, L. A.; Wang, L.; Matijevic, E. *Langmuir* **1998**, *14*, 4397.
(8) (a) Dai, Z. R.; Pan, Z. W.; Wang, Z. L. *Adv. Funct. Mater.* **2003**, *13*, 9. (b) Ramgir, N. S.; Mulla, I. S.; Vijayamohanan, K. P. *J. Phys. Chem. B* **2004**, *108*, 14815.
(9) Pinna, N.; Willinger, M.; Weiss, K.; Urban, J.; Schlogl, R. *Nano Lett.* **2003**, *3*, 1131.
(10) Steele, B. C. H. *Solid State Ionics* **2000**, *129*, 95.
(11) Laha, S. C.; Ryoo, R. *Chem. Commun.* **2003**, 2138.
(12) (a) Masui, T.; Fujiwara, K.; Machida, K. I.; Adachi, G. Y. *Chem. Mater.* **1997**, *9*, 2197. (b) Li, R. X.; Yabe, S.; Yamashita, M.; Momose, S.; Yoshida, S.; Yin, S.; Sato, T. *Solid State Ionics* **2002**, *151*, 235.
(13) (a) Beie, H. J.; Gnoerich, A. *Sens. Actuators B* **1991**, *4*, 393. (b) Jasinski, P.; Suzuki, T.; Anderson, H. U. *Sens. Actuators B* **2003**, *95*, 73.
(14) Pemba-Mabiala, J. M.; Lenzi, M.; Lenzi, J.; Lebugle, A. *Surf. Interface Anal.* **1990**, *15*, 663.

10.1021/cm0507967 CCC: $30.25
Published on Web 07/22/2005

Table 1. Summary of Experimental Conditions

morphology	cerium precursor concentration	reaction time (h)
spheres	80 mM	4
rods	80 mM	24
spindle-like	40 mM	24

in electronic conductivity in CeO_2 nanocrystals compared to micrometer-sized coarse grain.[15] Due to the quantum size effect, a blue shift in UV absorption spectrum was observed.[16] The rate of CO oxidation on gold deposited on nanocrystalline particles of cerium dioxide was found to be a hundred times higher than that of Au on regular CeO_2 support.[17] The development of preparation methods to control the morphology of CeO_2 is needed for tapping the full potential of CeO_2. Nevertheless, only a few reports have emerged about the fabrication of 1D cerium compound nanostructures. These include the synthesis of cerium compound nanowires and nanorings templated by NaAOT (sodium bis(2-ethylhexyl)sulfosuccinate) and alkyl alcohol as well as the formation of cerium dioxide nanowires from a mixture of cerium acetate and NaAOT.[18] We report for the first time the synthesis of cerium dioxide nanospheres, spindle-like and rod-shaped microparticles via a simple solution route. The morphology can be controlled by simply changing the reaction time and the concentration of the cerium precursor. Moreover, the correlations between the band gap energies, grain size, and morphology of the samples have been studied.

2. Experimental Section

2.1. Materials and Experimental Conditions. Chemical reagents including ammonium cerium (IV) nitrate ($[(NH_4)_2Ce(NO_3)_6]$, Acros), ethylene glycol (EG, Panreac), and poly(vinylpyrrolidone) (PVP M_w 10000, Aldrich) were used as received without further purification. Table 1 shows the appropriate concentrations of ammonium cerium(IV) nitrate ($[(NH_4)_2Ce(NO_3)_6]$) required for the preparation of CeO_2 nanospheres and rod-shaped and spindle-like particles. The cerium precursor was dissolved in 30 mL of ethylene glycol containing 0.16 M PVP under vigorous stirring until a homogeneous colorless solution was obtained. The mixture was heated under reflux to the boiling point of ethylene glycol (ca. 190 °C) for either 4 or 24 h (Table 1). The color of the solution changed initially to yellowish brown and a brown gas was evolved during reflux. A white precipitate started to appear after about 2 h and the reaction mixture became milky. At the end of the predetermined reaction time, the mixture was centrifuged and washed with deionized water and absolute ethanol to remove excess ethylene glycol and PVP. After drying overnight in a vacuum oven at 80 °C, the product was calcined at 600 °C for 4 h for crystallization.

We also prepared another ceria catalyst support by a coprecipitation method. $(NH_4)_2Ce(NO_3)_6$ was dissolved in deionized water to give a clear orange solution. Then the resulting solution was added dropwise to ammonia (35%). The yellow hydrated precipitates were filtered off and dried at 80 °C. Finally, the dried product was calcined at 600 °C for crystallization.

2.2. Characterizations. Powder X-ray diffraction data were recorded by using a Bruker D8 Advance X-ray diffractometer with Cu Kα_1 irradiation ($\lambda = 1.5406$ Å) at a scanning rate of 0.01°/s. The crystal size was estimated by applying the Schrerrer equation ($\Phi = K\lambda/\beta \cos\theta$), where Φ is the crystal size, λ is the wavelength of the X-ray irradiation (0.154 nm), K is usually taken as 0.89, β is the peak width at half-maximum height after subtraction of the instrumental line broadening using silicon as a standard, and θ is the diffraction angle of the (111) peak of the cubic phase. Scanning electron microscopy (SEM) measurements were carried out on a LEO 1450VP scanning microscope to investigate the morphology and surface roughness of samples. Transmission electron microscopy (TEM) and high-resolution transmission electron microscopy (HRTEM) images were recorded on a Tecnai 20 FEG microscope. A trace amount of sample was suspended in ethanol solution, followed by sonication for 10 min. Carbon-coated copper grids were used as the sample holders.

Nitrogen adsorption−desorption isothermals were collected at 77 K using Micromeritics ASAP 2010 equipment (BET and BJH models, respectively, for specific surface area and porosity evaluation). All the samples were degassed at 150 °C and 10^{-6} Torr for 24 h prior to the measurement. Surface composition was determined by X-ray photoelectron spectroscopy (XPS) using a PHI Quantum 2000 XPS System with a monochromatic Al Kα source and a charge neutralizer. All the binding energies were referenced to the C 1s peak at 284.8 eV of the surface adventitious carbon.

The solvent of the reaction mixture was analyzed by gas chromatography−mass spectrometry (GC/MS) to detect the intermediates produced from the reactions between ethylene glycol and $(NH_4)_2Ce(NO_3)_6$ under the high temperature. A HP 6890 GC system equipped with a HP-5MS (30 m × 0.25 mm × 0.25 μm (5%-phenyl)-methylpolysiloxane) column and a HP 5973 Mass Selective Detector was used in the study. Before GC/MS analysis, the sample was centrifuged to remove the particles from the solution. Two hundred fifty microliters of the sample and 250 μL of chloroform were then transferred into a glass vial and dried in an oven for 5 days at 55 °C. The organic residue was diluted in chloroform with the addition of 50 μL of naphthalene standard. It was then sonicated for 30 min and transferred to 1.5 mL amber vials with screw caps. One microliter of the sample was manually injected for analysis. The initial temperature was maintained at 70 °C for 3 min, then increased to 160 °C at a rate of 80 °C min^{-1}, and then gradually raised to 250 °C at a rate of 2 °C min^{-1}. The solvent delay was 3.5 min. The flow rate of helium carrier gas was 1.0 mL min^{-1}. The MS transfer line temperature was set as 280 °C. Mass spectra were recorded by standard electron ionization (70 eV) at the EI mode. The total GC run time was 60 min. The MS detector was operated in full scan mode, scanning between m/z 35 and m/z 700 repeatedly during each GC run. Interpretation of mass spectra was supported by literature data and NIST spectra library.

The FT-IR spectra of the samples were obtained on a Nicolet FT-IR 560 FT-IR spectrometer. The UV−Vis spectra of the samples were recorded on a Cary 100 a UV−Vis spectrophotometer using a quartz cell (1 cm path length). The calcined CeO_2 nanospheres and rod-shaped and spindle-like particles were each dispersed in ethanol at a concentration of about 10^{-3} mol L^{-1} and then sonicated for 1 h to obtain transparent colloidal solutions. The UV−Vis absorption spectra were recorded using pure ethanol as a blank and spectral grade $BaSO_4$ powder as a reference.

(15) Chiang, Y. M.; Lavik, E. B.; Kosacki, I.; Tuller, H. L.; Ying, J. Y. *Appl. Phys. Lett*. **1996**, *69*, 185.
(16) Zhang, Y. W.; Si, R.; Liao, C. S.; Yan, C. H.; Xiao, C. X.; Kou, Y. *J. Phys. Chem. B* **2003**, *107*, 10159.
(17) Carrettin, S.; Concepcion, P.; Corma, A.; Lopez Nieto, J. M.; Puntes, V. F. *Angew. Chem., Int. Ed.* **2004**, *43*, 2538.
(18) (a) Yada, M.; Sakai, S.; Torikai, T.; Watari, T.; Furuta, S.; Katsuki, H. *Adv. Mater*. **2004**, *16*, 1222. (b) Sun, C.; Li, H.; Wang, Z. X.; Chen, L.; Huang, X. *Chem. Lett.* **2004**, *33*, 662. (c) Wu, G. S.; Xie, T.; Yuan, X. Y.; Cheng, B. C.; Zhang, L. D. *Mater. Res. Bull*. **2004**, *39*, 1023.

CeO_2 nanospheres and rod-shaped and spindle-like samples were selected as the catalysts for CO oxidation. Catalytic tests were carried out in a conventional fixed-bed quartz microreactor (8 mm in outer diameter) between 50 and 140 °C with the feeding of 0.2 g of sample diluted with 0.2 g of silica gel. The catalysts were activated in a flow of air (80% N_2 and 20% O_2, 50 mL min^{-1}) at 400 °C for 2 h and cooled to desired temperatures. A gas mixture (1% CO, 20% O_2, and 79% N_2) was then introduced into the reactor at a flow rate of 50 mL min^{-1}. The reaction mixtures were analyzed on-line by gas chromatography using a Porapak Q column for the separation of CO and CO_2 and a 5A Molecular Sieve column for the separation of O_2 and N_2. The conversion of CO to CO_2 over the catalysts was measured at various temperatures. T_{50} and T_{90} are defined as the temperatures at which the conversion of CO to CO_2 reached 50 and 90%, respectively.

3. Results and Discussion

3.1. SEM and TEM Analysis. Various shapes of CeO_2 nanoparticles were prepared by mixing $(NH_4)_2Ce(NO_3)_6$ and ethylene glycol, by varying the concentration of the cerium precursor and the duration of the reaction. The optimal reaction conditions for the formation of CeO_2 nanospheres and rod-shaped and spindle-like samples are summarized in Table 1. The morphology of the obtained CeO_2 nanocrystals was examined by scanning electron microscope (SEM) and transmission electron microscope (TEM). Representative SEM and TEM micrographs of annealed CeO_2 nanospheres are shown in Figures 1a−c. These figures reveal monodispersed nanospheres with a relatively uniform diameter of 80−100 nm. The electron diffraction (ED) pattern (inset of Figure 1b) confirms the polycrystalline nature of the sample and its face-centered cubic crystal structure. These results are consistent with that obtained by XRD (Figure 2a). From the ED pattern, it can be concluded that the CeO_2 nanospheres are built up from the aggregation of small crystallites. The energy-dispersive X-ray spectroscopy (EDX) measurements confirm that the nanospheres are composed of Ce and O in the ratio of 1:2 (Figure 1d).

The SEM and TEM images of the annealed CeO_2 rod-shaped samples synthesized with different reaction times are shown in Figures 1e and f, respectively. When the reaction media was heated for 24 h, samples were obtained with widths of several hundred nanometers and lengths ranging between 15 and 20 μm (based on SEM/TEM image estimations). A large aspect ratio is thus achieved in the range of 25 to 33. Furthermore, each microrod shows a highly uniform diameter. From the enlarged image, both ends of the sample are needle-shaped. The HRTEM image (Figure 1g) indicates clearly that they are composed of many tiny grains with different orientations. The spacing between two adjacent lattice planes is 0.313 nm, which corresponds to the separation of the (111) lattice planes of CeO_2 (Figure 1g).

Representative SEM and TEM images of the spindle-like particles are shown in Figures 1h and i. When refluxed for 24 h, spindle-like particles are formed with widths of several hundred nanometers and lengths ranging from 2 to 4 μm and aspect ratios of 4−8. Moreover, each spindle-like nanoparticle shows sharp-ends and curved edges. The width of these samples increases from the ends to the center. The widths of rod-shaped and spindle-like particles are similar, but they differ in length. A careful look from the end elevation of spindle-like particles reveals pyramid-like ends with sharp edges (the insets in Figures 1h), whereas rod-shaped samples have spin-like ends. To study the growth process of this rod-shaped structure, an aliquot of the reaction mixture was withdrawn at 4, 8, 12, and 16 h. As illustrated in Figures S1a−d, rods and nanospheres coexisted in the reaction mixture after 8 h of reflux, but neither small-size nanorods nor preformed product can be observed. This may suggest that the microrods are not grown from the aggregation of nanospheres. In fact, the amount of microrods increased with duration of the reaction. However, the length and width of the microrods are independent of reaction time and refluxing temperature. After a 16-h reaction, over 90% of the products is microrods (estimated from the SEM micrograph) with just a small amount of nanospheres.

The above-mentioned investigations reveal that the morphology of CeO_2 nanoparticles is controlled by the concentration of cerium precursor and reaction duration. To study the growth mechanism, X-ray diffraction (XRD), Fourier transform infrared spectroscopy (FT-IR), and X-ray photoelectron spectroscopy (XPS) were used to characterize the as-prepared sample and the calcined sample.

3.2. XRD Analysis. Phases and purities of the as-prepared samples were investigated by the XRD analysis. Figure 2a shows the XRD patterns of the as-prepared CeO_2 nanospheres. All the diffraction peaks can be indexed as a face-centered cubic-phase CeO_2 (JCPDS 34-0394). The lattice parameters calculated from this pattern ($a = b = c = 3.12$ Å) are in accordance with the reported values. Surprisingly, diffraction patterns for the microrods and spindle-like structures are completely different from those for the nanospheres (Figures 2b and c). Based on the XRD patterns, the microrods and spindle-like particles have the same crystal structure and can be identified as cerium formate (JCPDS 49-1245, $Ce(HCOO)_3$). The as-prepared samples are free of impurities and there is no trace of the precursor.

All samples maintain their original morphology but they all exhibit face-centered cubic lattice structure after calcination at 600 °C for 4 h (Figure 3). The diffraction peaks match that of a face-centered cubic-phase CeO_2 reported in JCPFS (34-0394). The lattice parameters calculated from these patterns are summarized in Table 2. A closer observation of the reflection peak (111) at ca. 28.5° (Figure 4) reveals that there is a slight downshift from the nanospheres to microrods and spindle-like particles with a corresponding increase in the unit cell volumes (Table 2).

3.3. N_2 Sorption. Physicochemical properties of as-prepared and annealed samples are listed in Table 3. Interestingly, both surface area and pore volume increased after calcination. The surface area of CeO_2 nanospheres shows a 4-fold increase while that of other samples (microrods and spindle-like particles) also increase significantly. Before calcination, the cerium formate repeating units are linked together through the organic-based bridge to give a 1D dimensional structure. High-temperature treatment breaks the bridging units and initiates the crystallization of the repeating units. The secondary structure of calcined nanospheres and rod or spindle-like shape can be considered as

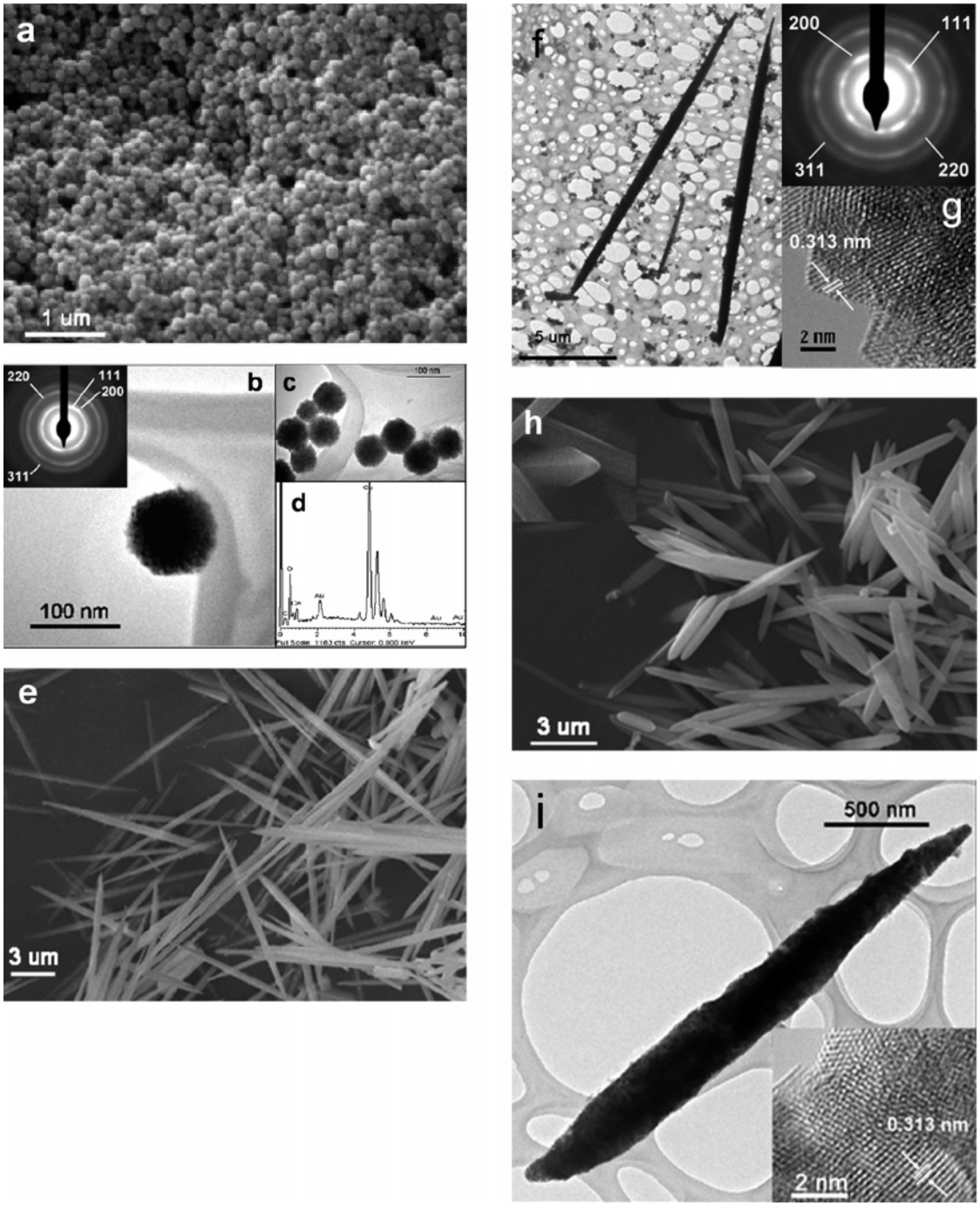

Figure 1. (a) SEM images of annealed CeO_2 nanospheres at 600 °C for 4 h HRTEM: (b), (c) CeO_2 nanospheres TEM images and its electron diffraction pattern (inset), (d) EDX of nanospheres shows the ratio of Ce:O ≈ 2:1, (e) SEM and (f) TEM images of annealed CeO_2 microrods at 600 °C for 4 h, (g) HRTEM image of the selected area of the CeO_2 microrods, (h) SEM image of CeO_2 spindle-like particles and (g) TEM and HRTEM images (inset) of individual particles.

the agglomeration of each primary nanoparticle. Therefore, the surface area and the pore volume greatly increased after calcinations. The nitrogen adsorption−desorption isotherms and the Barrett−Joyner−Halenda (BJH) pore size distributions for as-prepared and calcined nanospheres, microrods, and spindle-like structures are shown in Figures S2−4. From Figure S3a, two distinct capillary condensation steps appear at P/P_o values of about 0.5 and 0.8, respectively. BJH model analysis of these as-prepared microrods gives one narrow peak centered at 5 nm in the pore size distribution and another broad peak in the range of 10−20 nm with an evident maximum at 13 nm, showing a dual mesoporous distribution. The desorption branch also displays two distinct steps. This suggests that two pore systems with different diameters are present to form a three-dimensional pore structure. A similar pattern can also be observed in the as-prepared spindle-like particles (Figure S4a). Two distinct capillary condensation steps also can be observed at P/P_o values of about 0.45 and 0.8, respectively, from Figure S4a. A narrow peak centered at 3.5 nm and another broad peak in the range of 10−20 nm with an evident maximum at 14 nm in pore distribution clearly suggests a bimodal porosity distribution. The isotherms for both samples are apparently of type IV, typical of mesoporous materials. These results confirm the formation

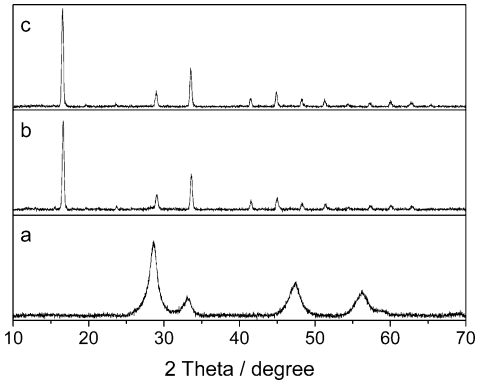

Figure 2. XRD pattern for as-prepared samples: (a) CeO_2 nanospheres, (b) rod-shaped precursor $Ce(HCOO)_3H_2O$, and (c) spindle-like particles $Ce(HCOO)_3H_2O$ precursor.

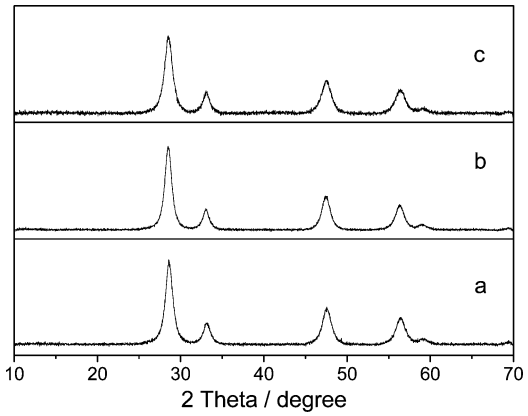

Figure 3. XRD pattern for calcined CeO_2 samples: (a) nanospheres, (b) microrods, and (c) spindle-like particles.

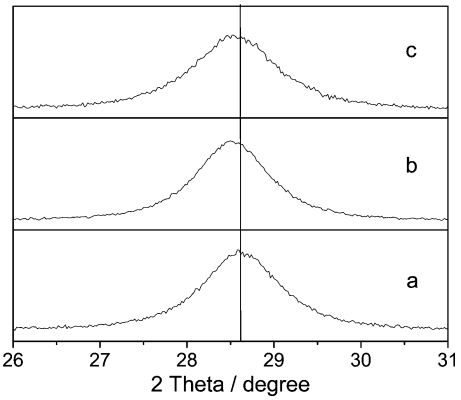

Figure 4. XRD spectra ($2\theta = 26°-31°$) for annealed samples: (a) nanospheres, (b) microrods, and (c) spindle-like particles.

Table 2. Summary of the Lattice Parameter *d*, Interatomic Distance *a*, Lattice Volume *V*, and Crystal Size

morphology	2θ	*d* (Å)	*a* (Å)	*V* (Å^3)	crystal size (nm)
spheres	28.61	3.118	5.400	157.5	8.97
rods	28.52	3.127	5.416	158.8	8.41
spindle-like	28.51	3.128	5.419	159.0	7.60

of the bimodal mesoporous cerium microrods and spindle-like particles.

3.4. X-ray Photoelectron Spectroscopy. Ce 3d electron core level XPS spectra for as-prepared and calcined nanospheres, microrods, and spindle-like particles are shown in Figures 5a−c. The 3d level is formed by two series of peaks: $3d_{5/2}$ and two very pronounced "shake-up" satellites

Table 3. Physicochemical Properties of the As-Prepared and Annealed Samples

shape of the samples	S_{BET}[a] (m^2/g)	V[b] (cm^3/g)	D_{BJH}[c] (nm)
spheres (as-prepared)	40.3	0.077	7.6
spheres (calcined)	158.2	0.23	5.8
rod (as-prepared)	67.8	0.13	7.8
rod (calcined)	145.0	0.20	5.6
spindle-like (as-prepared)	67.4	0.11	7.1
spindle-like (calcined)	170.0	0.19	4.4

[a] BET surface area calculated from the linear part of the BET plot ($P/P_0 = 0.1-0.2$). [b] Total pore volume, taken from the volume of N_2 adsorbed at $P/P_0 = 0.995$. [c] Average pore diameter, estimated using the desorption branch of the isotherm and the Barrett−Joyner−Halenda (BJH) formula.

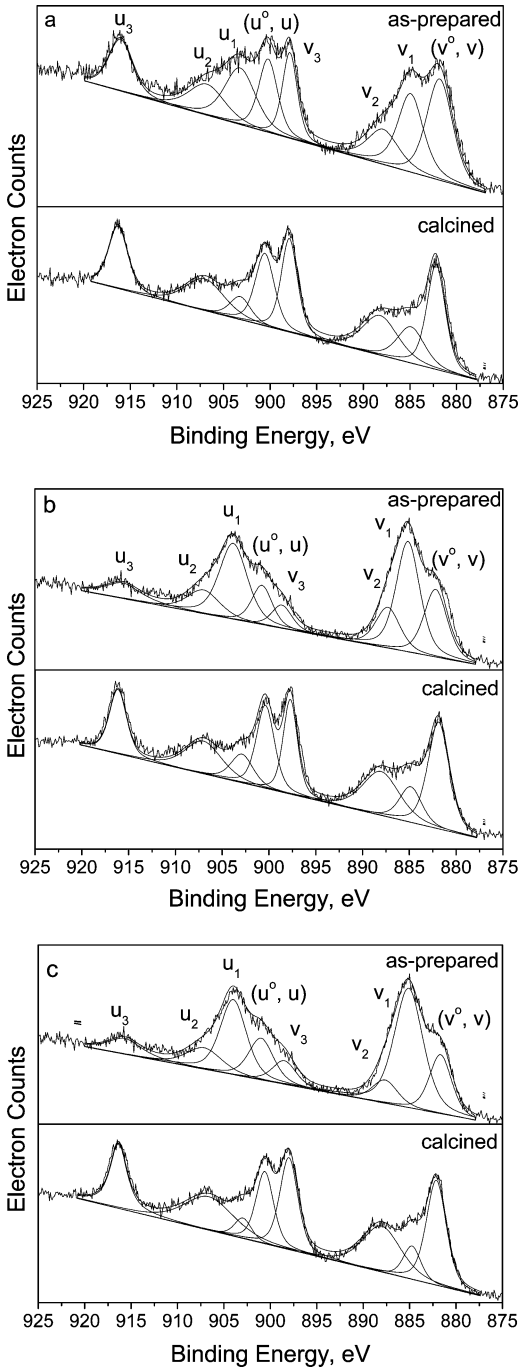

Figure 5. XPS spectra for as-prepared and annealed CeO_2 sample: (a) nanospheres, (b) microrods, and (c) spindle-like particles.

and $3d_{3/2}$ with the same characteristics. The peaks labeled v and v_2 have been assigned to a mixing of the Ce $3d^9$ $4f^2$

L^{n-2} and Ce $3d^9$ $4f^1$ L^{n-1} Ce(IV) final states, and the peak denoted v_3 corresponds to the Ce $3d^9$ $4f^0$ L^n Ce(IV) final state. Moreover, lines v_0 and v_1 are assigned to the Ce $3d^9$ $4f^2$ L^{n-1} and Ce $3d^9$ $4f^1$ L^n states of Ce(III). The same assignment can be applied to the u structures, which correspond to the Ce $3d_{3/2}$ levels.[19] The Ce3d XPS spectra of as-prepared microrods and spindle-like structures are very different from those of the CeO_2 nanospheres. The increasing intensity of the u_1, v_1 band and reduction of the other bands in as-prepared cerium microrods and spindle-like particles strongly suggest that the oxidation state of cerium is mainly from Ce(III) (Figures 5b and c). The energy separation between the v and v_1 peaks is about 3.0 eV, close to the values observed for Ce(III) compounds.[20] As compared with the XPS spectra for as-prepared and calcined cerium nanospheres (Figure 5a), an increase in band intensities of u_1 and v_1 reveals that cerium is already in a partially reduced form. This is because the reaction with CeO_2 and ethylene glycol leads to partial reduction of Ce(IV). The relatively high intensity of other Ce(IV) lines leads to the conclusion that both Ce(III) and Ce(IV) coexisted in the nanosphere structure before calcination. Based on the relative intensity of Ce(IV) and Ce(III) lines, as-prepared nanospheres should mainly be built up from Ce(IV) nanocrystals. After high-temperature calcination, the sharp decrease in u_1 and v_1 lines and increase in other Ce(IV) lines reveals that all the cerium in samples convert to Ce(IV) as the final oxidation state. Therefore, the XPS and XRD results indicate that ammonium cerium nitrate first decomposes to cerium (IV) oxide and further reduces to cerium (III) formate by ethylene glycol. Reaction of ethylene glycol and cerium (III) formate induces the 1D morphology formations.

3.5. FT-IR Analysis. Figure 6a shows the FT-IR spectra for the as-prepared and calcined cerium microrods and spindle-like structures. The typical peaks for metal formate salt are found at ca. 1600, 1360, and 775 cm^{-1}. The first two frequencies correspond to the stretching mode of C═O in an oxalate group and the last one refers to its bending mode. The absence of the Ce−O stretching band at ca.400 cm^{-1} confirms that the as-prepared microrods and spindle-like particles are not composed of CeO_2. It should also be noted that no C−H stretching peaks (2800 to 2900 cm^{-1}) can be found in the FT-IR spectra, which is different from that reported by Xia et al. for the formation of titanium dioxide nanowires from titanium alkoxide.[4a,b] In the case of TiO_2, the 1D morphology is put together by the linking action of ethylene glycol to yield repeating units of (O−CH_2CH_2−O−M). In the present study, the repeating units are cerium formate.

After calcination, only the Ce−O stretching band remains at ca. 400 cm^{-1}, indicating the structural transformation to CeO_2 from the cerium formate as-prepared compound. The peak at ca. 3400 cm^{-1} corresponds to the physically adsorbed water on the sample. As compared with the nanospheres (Figure 6b), the disappearance of the peaks corresponding to C═O in oxalate group confirms the different formation mechanisms in nanospheres and microrods. The creation of spherical particles should be mainly due to the capping action by PVP. This can also be supported by the appearance of C−N (1560 cm^{-1}) and C═O (1660 cm^{-1}) stretching frequency from the disubstituted amide group in FT-IR studies. Both FT-IR spectra for as-prepared and calcined samples show absorption peaks at 400 to 450 cm^{-1} and reveal that as-prepared samples are structurally combined as CeO_2.

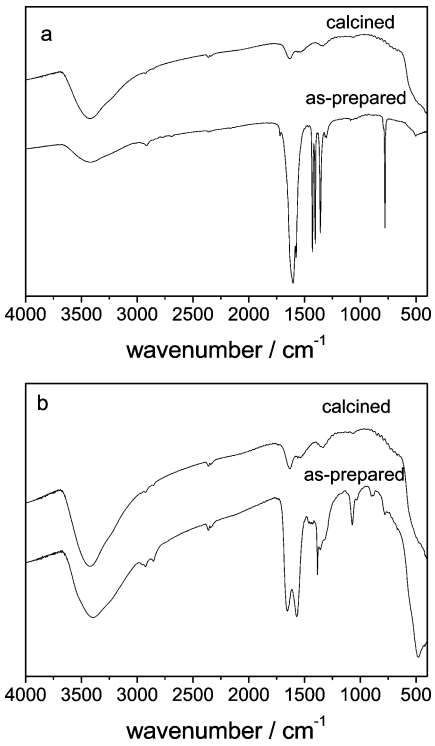

Figure 6. FT-IR spectra for (a) rod-shaped and spindle-like shaped sample and (b) nanospheres.

3.6. GC-MS Analysis. To study the reaction between ethylene glycol and ammonium cerium nitrate, 2 mL of the reaction mixture was withdrawn and analyzed at certain time intervals during reflux. Samples were centrifuged and a clear pale yellow solution was obtained. The content of the reaction mixture was analyzed by GC-MS. A polymerization product of ethylene glycol can be found in the GC chromatograph after 2 h (Figure S5a). This compound with a retention time of 5.646 min has been identified by MS (Figure S6a). The product, 2-[2-(2-hydroxyethoxy)ethyoxy]-ethanol, was formed by the polymerization reaction of ethylene glycol under high temperature. Xia et al. also suggested that the bridging unit of the 1D SnO_2 nanowires came from the polymerization of ethylene glycol. The other two peaks positioned at 5.193 and 5.456 min correspond to a smaller polymer of ethylene glycol and head of PVP (Figures S6b and c). After further heating reflux for 4, 8, and 10 h (Figure S5b−d), oxalic acid appeared as a peak positioned around 5.4 min (Figure S6d). It was a surprise that the peak height of the oxalic acid increased with the reaction time and it was indicated that there was more ethylene glycol molecule oxidized to oxalic acid (Figure

(19) (a) Nelson A. E.; Suhulz, K. H. *Appl. Surf. Sci.* **2003**, *210*, 206. (b) Pfau A.; Schierbaum, K. D. *Surf. Sci.* **1994**, *321*, 71. (c) Kulkarni, G. U.; Rao, C. N. R.; Roberts, M. W. *J. Phys Chem.* **1995**, *99*, 3310. (d) Kotani, A.; Mizuta, H.; Jo T.; Parlebas, J. C. *Solid State Commun.* **1985**, *53*, 805. (e) Wuilloud, E.; Delley, B.; Schneide W. D.; Baer, Y. *Phys. Rev. Lett.* **1984**, *53*, 202.
(20) Shyu, J. Z.; Weber, W. H.; Gandhhi, H. S. *J. Phys. Chem.* **1988**, *92*, 4964.

S5e). From XRD analysis, it is clearly shown that the product obtained at the beginning was CeO_2 nanospheres and cerium formate compound was formed after 24 h. $(NH_4)_2Ce(NO_3)_6$ was decomposed to CeO_2 nanospheres in the first few hours of reaction. These CeO_2 nanospheres further reacted with ethylene glycol to give the cerium formate compound eventually. The gradual increase in the amount of oxalic acid suggests that the rate for the transformation of CeO_2 nanospheres to cerium formate may be dependent on the amount of oxalic acid. It is clearly shown in Figure S1 that no cerium formate microrods were formed at the early stage. They begin to appear only when oxalic acid becomes available in the reaction system.

3.7. Proposed Formation of CeO_2 Nanospheres and Their Transformation to Microrods. The cerium dioxide nanospheres are formed from the decomposition of ammonium cerium nitrate at temperatures above 185 °C:

$$(NH_4)_2Ce(NO_3)_6 \rightarrow 4H_2O + 2N_2O + 4NO_2 + O_2 + CeO_2\downarrow \text{(nanospheres)}$$

The spherical morphology results from the capping action of the surfactant PVP.[4f] The gradual transformation of nanospheres to microrods is illustrated in Figures S1a−d. These SEM images reveal that the microrods are not assembled by the aggregation of the nanospheres. We believe the growth process starts with the reaction between the nanospheres and ethylene glycol. Ethylene glycol is an alcohol with a pK_a value of about 15.[21] It can be oxidized to carboxylic acids in the presence of oxidant, ammonium cerium nitrate, as shown in the following reactions:[21]

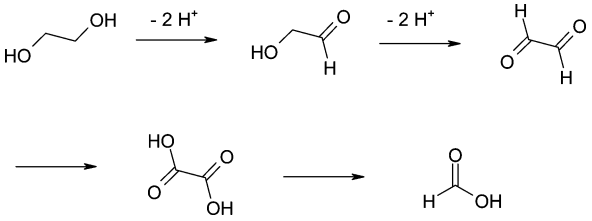

The oxidation of the alcohol groups gives aldehydes and then oxalic acid and formic acid. The presence of oxalic acid in the reaction mixture has been confirmed by GC-MS analysis (Figures S5d and S6d). Meanwhile, the cerium(IV) cations in CeO_2 are reduced by ethylene glycol to cerium(III). The Ce^{III} ion centers interact with the carboxylic groups in formic acid to yield cerium formate. The cerium formate acts as building blocks that are linked together to form the 1D microrods and spindle structures. However, the formate groups cannot be the bridging units due to a strong steric hindrance effect. The FTIR and GC-MS results reveal that the bridging unit is oxalic acid which comes from the oxidation of ethylene glycol. Each cerium formate unit reacts with oxalic acid to form a long chain. During the reaction, one of the formate groups of $Ce(HCOO)_3$ is substituted by an oxalate unit and the two remaining formate groups are arranged in a *trans*-geometry. The proposed formation mechanism is as follows:

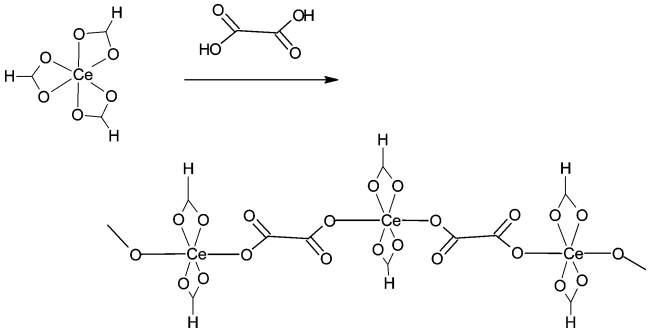

During calcination, the cerium formate nanostructures are oxidized to cerium dioxide.

3.8. UV Absorption Spectra and Band Gap Energies. To reveal the correlation between the band gap energies and the grain size and morphology of the sample, the UV−Vis absorption spectra of calcined CeO_2 nanospheres, microrods, and spindle-like particles were recorded. The optical absorption coefficient α was calculated according to the following equation: $\alpha = (2.303 \times 10^3 A\rho)/lc$, where A is the absorbance of the sample, ρ is the real density of CeO_2 (7.28 g cm^{-3}), l is the path length of the quartz cell (1 cm), and c is the concentration of the ceria suspensions.[16] The UV−Vis absorption spectra of the cerium dioxide nanospheres, microrods, and spindle-like structures were measured in ethanol suspensions (Figure S7). Both of them exhibit strong absorption bands at ca. 270 and 340 nm in the UV range, which originate from the charge-transfer between the O2p and Ce4f states in O^{2-} and Ce^{4+}.[22] This spectral profile indicates the charge-transfer transition of Ce^{4+} overlaps with the $4f^1 \rightarrow 5d^1$ transition of Ce^{3+}. No absorption was detected above 500 nm in wavelength. A clear blue-shifting of the absorption threshold edge can be observed for the CeO_2 nanospheres and microrods, contrasting with the bulk powder. The plots of $(\alpha h\nu)^2$ vs photon energy of CeO_2 nanospheres, microrods, and spindle-like particles are shown in Figure 7. For direct transitions, the absorption coefficient near the absorption edge can be expressed in the following equation: [23]

$$\alpha \propto \frac{\sqrt{h\nu - E_d}}{h\nu}$$

where E_d is the band gap energy for direct transitions and $h\nu$ is the photon energy. From the intersection of the extrapolated linear portion, the E_d values of the CeO_2 nanospheres, microrods, spindle-like particles, and bulk samples can be determined as 3.46, 3.62, and 3.36 eV, respectively. Compared to the nonoriented polycrystalline CeO_2 ($E_d = 3.19$ eV determined by UV−vis spectroscopy),[24] CeO_2 nanospheres, microrods, and spindle-like structures showed an increase in E_d by a value exceeding 0.27, 0.43, and 0.17 eV, respectively. The blue-shifting phenomenon in the UV absorption spectra of CeO_2 nanocrystals has

(21) Bock, C.; Paquet, C.; Couillard, M.; Botton, G. A.; MacDougall, B. R. *J. Am. Chem. Soc.* **2004**, *126*, 8028.

(22) (a) Tsunekawa, S.; Fukuda, T. *J. Appl. Phys.* **1999**, *87*, 1318. (b) Tsunekawa, S.; Sahara, R.; Kawazoe, Y.; Kasuya. A. *Mater. Trans. JIM* **2000**, *41*, 1104.

(23) Van Leeuwen, R. A.; Huang, C. J.; Kammler, D. R.; Switzer, J. A. *J. Phys. Chem. B* **1995**, *99*, 15247.

(24) Orel, Z. Z.; Orel, B. *Phys. Status Solidi B* **1994**, *186*, K33.

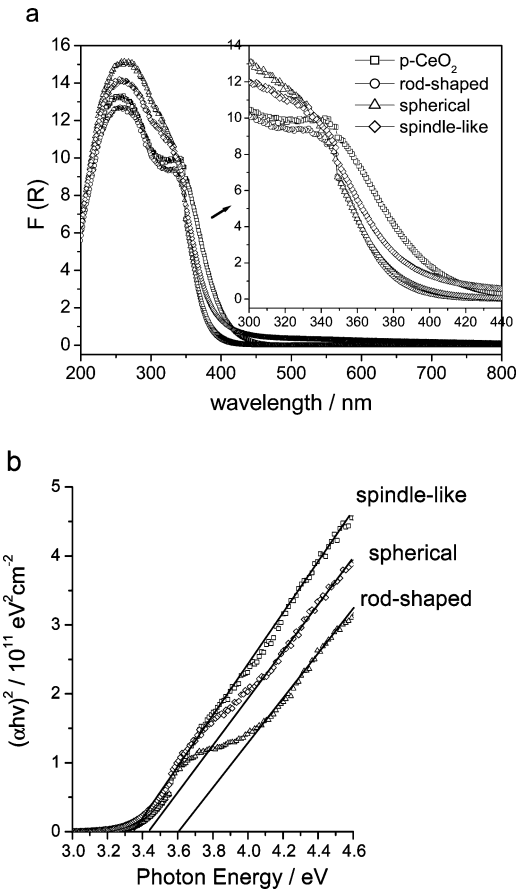

Figure 7. (a) UV spectra for annealed CeO_2 nanospheres, microrods, and spindle-like particles; (b) plots of $(\alpha h\nu)^2$ vs photon energy for the annealed samples.

attracted the interest of many researchers in recent years.[25] Generally, the absorption of ceria in the UV region originates from the charge-transfer transition between the O 2p and Ce 4f states in O^{2-} and Ce^{4+}. This absorption is much stronger than the $4f^1-5d^1$ transition from the Ce^{3+} species in the mixed valence ceria system.[22,25c] It was theoretically deduced that the value of blue-shifting resulting from the reduction of particle size is inverse proportional to the square of the size due to quantum confinement effect. Tsunekawa et al. stated that the blue shifts could also be explained by changes in the electronic band structure.[25d]

3.9. Thermal Catalysis Study. The spherical, rod-shaped, and spindle-like annealed CeO_2 samples as well as a reference sample ($P-CeO_2$) were tested for their ability to oxidize carbon monoxide:

$$CO + {}^1/_2O_2 \rightarrow CO_2$$

Figure 8 shows the catalytic activity profiles of CO conversion for the samples. The results of the catalytic activity measurements are summarized in Table 4. The spindle-like sample shows the highest CO conversion rates 0.861 μmol g^{-1} s^{-1}, which is almost 4.5 times that for our reference

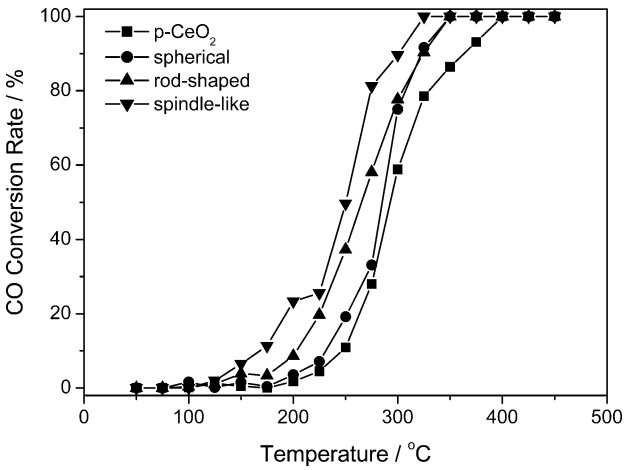

Figure 8. CO conversion as a function of temperature over CeO_2 nanospheres, microrods and spindle-like particles.

Table 4. Summary of Results from CO Oxidation Measurements

	T_{50} (°C)	rate (μmol g^{-1} s^{-1})	E_a (kJ mol^{-1})
P-CeO_2	294	0.189 (250 °C), 1.019 (300 °C)	69.80
spherical	284	0.332 (250 °C), 1.300 (300 °C)	57.55
rods	265	0.646 (250 °C), 1.347 (300 °C)	43.44
spindle-like	250	0.861 (250 °C), 1.554 (300 °C)	52.55

$P-CeO_2$, 0.189 μmol g^{-1} s^{-1}. The large difference in catalytic activity is partly due to the variation in surface area. The surface area of the spindle-like sample is 170.0 m^2/g but that of $P-CeO_2$ calcined at 600 °C is only 65.3 m^2/g.

Interestingly, the surface area and pore volume for the three types of samples are almost the same (Table 3) but the spindle-like and rod-shaped samples show much higher catalytic activities than the nanospheres. XRD analysis indicates that the order of lattice cell volume is spindle-like $\approx$ rod-shaped $>$ spherical (Table 2) and the lattice cell expansion is strongly related to the degree of Ce(IV) reduction and the extent of oxygen vacancy.[26] In addition to the surface area, structural defects and oxygen vacancy also have a positive effect on CO oxidation.[26] The formation of oxygen vacancy can be expressed by the following equation:

$$4Ce^{4+}{}_{(s)} + O^{2-}{}_{(s)} \rightarrow 4Ce^{4+} + 2e^-/V_{(O,s)} + {}^1/_2O_2 \rightarrow 2Ce^{4+}, 2Ce^{3+}{}_{(s)} + V_{(O,s)} + {}^1/_2O_2$$

where $V_{(O,s)}$ represents an empty position (anion-vacant site) originating from the removal of O^{2-} from the lattice. Charge balance is maintained by the reduction of two cerium cations from +4 to +3. The radius of the Ce^{3+} ion (1.14 Å) is larger than that of Ce^{4+} (0.97 Å) and hence the lattice expansion is a consequence of the reduction of Ce^{4+} ions to Ce^{3+}.[27] There is a gradual decrease in the concentration of oxygen vacancies extended from the surface to the bulk. Such gradient enables the outward diffusion of lattice oxygen to the surface. Therefore, reduction of Ce^{4+} to Ce^{3+} by oxygen ion leads to the generation of surface oxygen vacancy. These oxygen vacancies can act as promoting sites for NO and CO

(25) (a) Inoue, M.; Kimura, M.; Inui, T. *Chem. Commun*. **1999**, 957. (b) Yin, L. X.; Wang, Y. Q.; Pang, G. S.; Koltypin, Y.; Gedanken, A. *J. Colloid Interface Sci.* **2002**, *246*, 78. (c) Murata, T.; Sato, M.; Yoshida, H.; Morinaga, K. *J. Non-Cryst. Solids* **2005**, *351*, 312. (d) Tsunekawa, S.; Wang, J. T.; Kawazoe, Y.; Kasuya, A. *J. Appl. Phys*. **2003**, *94*, 3654.

(26) Trovarelli, A. *Catalysis by Ceria and Related Materials*; Imperial College Press: London, 2002; pp 15−50.

(27) Shannon, R. D.; Prewitt, C. T. *Acta Crystallogr. B*. **1969**, *25*, 925.

conversion. According to the lattice cell parameters in Table 2, we would expect the extent of Ce^{4+} reduction to be spindle-like ≈ rod-shaped > spherical. Fornasiero et al.[28] reported that the stress induced by the decrease of unit cell volume would create structural defects and generate oxygen vacancies. Moreover, the smaller crystalline size in the spindle-like particles also provides a larger percentage of atoms at the edges and corners (Table 2). The cerium and oxygen atoms at these locations are more chemically active.[29]

4. Conclusion

We have successfully fabricated uniform CeO_2 nanospheres, microrods, and spindle-like particles using a one-step procedure. Our results indicate that the morphology is controllable by the duration of reaction and the concentration of the cerium precursor. We believe that the decomposition of ammonium cerium nitrate and the redox reaction involving ethylene glycol leads to the growth of CeO_2 nanostructures. The band gap energies of these CeO_2 nanomaterials are shape-dependent (microrods > nanospheres > spindle-like particles). The higher catalytic activity on CO conversion in spindle-like particles can be explained from the extent of Ce(IV) reduction and the oxygen vacancy. This method is also applicable to the synthesis of mixed oxides ($Zr_xCe_{1-x}O_2$ and $Ti_xCe_{1-x}O_2$) nanoparticles. The simple preparation approach holds promise in the future large-scale synthesis of morphology-controllable CeO_2 for applications in solid electrolytes and electrochromic devices.

Acknowledgment. The work described in this paper was substantially supported by a grant from the Research Grants Council of the Hong Kong Special Administrative Region, China (Project No. 402904).

Supporting Information Available: Figure S1: SEM images of product obtained from the reaction mixture 80 mM $[(NH_4)_2Ce(NO_3)_6]$ in ethylene glycol with 0.16 M PVP heating reflux for (a) 4 h, (b) 8 h, (c) 12 h, and (d) 16 h. Figure S2: Nitrogen adsorption−desorption isotherms and BJH pore size distribution for (a) as-prepared and (b) calcined CeO_2 nanospheres. Figure S3: Nitrogen adsorption−desorption isotherms and BJH pore size distribution for (a) as-prepared and (b) calcined CeO_2 microrods. Figure S4: Nitrogen adsorption−desorption isotherms and BJH pore size distribution for (a) as-prepared and (b) calcined CeO_2 spindle-like particles. Figure S5: (a), (b), (c), (d), and (e) GC chromatographs of the solvent mixture after 2, 6, 8, 10, and 24 h of heating reflux. Figure S6: (a), (b), (c), and (d). The MS data for the compound with a retention time of 5.646, 5.193, 5.456, and 5.471 min. This material is available free of charge via the Internet at http://pubs.acs.org.

CM0507967

(28) Fornasiero, P.; Di Monte, R.; Ranga Rao, G.; Kaspar, J.; Meriani, S.; Trovarelli, A.; Graziani, M. *J. Catal.* **1995**, *151*, 168.
(29) (a) Burda, C.; Chen, X.; Narayanan, R.; El-Sayed, M. A. *Chem. Rev.* **2005**, *105*, 1025. (b) Di Monte, R.; Kaspar, J. *J. Mater. Chem.* **2005**, *15*, 633.